

A systematic method to develop three dimensional geometry models of buildings for urban building energy modeling

Chao Wang¹, Shen Wei², Sihong Du^{3,4}, Dian Zhuang¹, Yanxia Li¹, Xing Shi^{3,4,*}, Xing
Jin¹, Xin Zhou¹

¹School of Architecture, Southeast University, Nanjing, China, 210096.

²The Bartlett School of Construction and Project Management, University College
London, WC1E7HB, London, UK.

³College of Architecture and Urban Planning, Tongji University, Shanghai, China,
200092.

⁴Key Laboratory of Ecology and Energy-Saving Study of Dense Habitat, Ministry of
Education, Shanghai, China, 200092.

*Corresponding author: 20101@tongji.edu.cn

Abstract

Three dimensional (3D) geometric models of buildings are foundational for urban building energy modeling. A complete 3D geometric model contains building-relevant information like building footprint, height and Window-to-Wall Ratio (WWR). Existing methods creating these models have certain limitations, such as unavailability of Geographic Information System (GIS) databases and Light Detection and Ranging (LiDAR) data for many cities, and restricted flying space for Unmanned Aerial Vehicles

(UAV). To tackle these issues, this study has developed a systematic method developing 3D geometric models, with 1) building footprint acquired from combination of two internet maps, namely Baidu Map and OpenStreetMap; 2) building height estimated from the number of storeys for residential buildings and determined using the building vertical edge method for non-residential buildings, and 3) building WWR calculated from buildings' elevation images using an Artificial Intelligence (AI). The validation work revealed that more than 85% of acquired building footprints had absolute relative errors less than 10%, and this percentage was 87%, 74% and 75%, for height of residential buildings, height of non-residential buildings and WWR, respectively. To demonstrate the application of the method, a newly developed urban district in Nanjing, China was used as a case study.

Keywords: Urban building energy models, 3D models, geometric data, open-access data, GIS.

1. Introduction

Along with the rapid growth of both social population and economy, expansion of urban areas contributes greatly to global energy shortage and environmental deterioration [1-2]. It has been widely acknowledged that cities account for over 75% of the total energy consumption and carbon emissions of our society [3]. Due to this significant impact, in many major cities around the world, government has developed

long-term targets for energy conservation and Green House Gas (GHG) emission reduction. For example, San Francisco in the USA has set a target of reducing GHG emissions by 40% by 2025, comparing with the level in 1990 [4]. London in the UK is by 2025 aiming to reduce GHG emissions by 60% below the level in 1990 [5]. Both Beijing [6] and Shanghai [7] in China have set ambitions to reduce GHG emissions by 20.5% by 2020, compared with the level in 2015. To achieve these goals, city managers need to optimize local energy policies at urban levels, aided by planning tools providing both spatial and temporal energy data [8], especially for buildings, which are major energy consumers in cities [9-10].

To optimize urban energy usage, Urban Building Energy Models (UBEMs) have been developed to effectively calculate urban energy consumption and assist city managers to make decisions [11]. As a bottom-up, physical simulation model of heat and mass flows in and around groups of buildings, UBEMs are able to predict the energy consumption contributed by buildings within the urban level, as well as their indoor and local outdoor environmental conditions [8]. In addition to these, the models also help to explore opportunities for Energy Conservation Measures (ECMs) of a large group of buildings [12]. For example, Cerezo Davila et al. [13] have employed an UBEM approach to evaluate the energy efficiency of different scenarios in 172 houses in a city in Kuwait. In a case study carried out in San Francisco, Chen et al. [14] applied the UBEM in analyzing the energy and cost savings of five different ECMs for 940 office and retail buildings. A project targeting 3259 buildings in Lisbon was proposed by Monteiro et al. [15] to tap potential urban energy saving using UBEMs.

The development of UBEMs depends on the construction of a three dimensional (3D) geometry model for all individual building within the urban area under investigation, with information about their construction assemblies, occupancy, equipment and local climate [8]. A 3D model requires a large number of data to define the geometry of buildings, and these data can be categorized into three main groups, namely building footprint, building height and Window-to-Wall Ratio (WWR) [12]. CityGML¹ defines a 3D model representing at four Levels of Details (LODs), including (from LoD1 to LoD4): a box shape, adding slope roofs, adding exterior texture (like shades, windows and doors), and full details of interior layout and zoning [16]. A model LoD1 is derived from building footprints and heights. Owing to its simplicity and practicability [17], this kind of model has been widely used in developing UBEMs for many cities in the world, such as Boston [11], San Francisco [14], Cambridge [18], Amsterdam [19] and Gothenburg [20].

When constructing 3D geometry models for UBEMs, the most straightforward approach is to use the CityGML data. As reported by CityGML official [16], some cities, like Berlin, Rotterdam, Montreal and New York, have already open this kind of data to the public. However, it is either difficult to access or unavailable in most cities in other countries, which limits the development of local UBEMs.

Since a model LoD1 is composed of building footprints and heights, existing Geographic Information Systems (GIS) databases, which contain useful data for many

¹ CityGML, an international Open Geospatial Consortium (OGC) standard that provides an open data model to represent and exchange digital 3D models of cities and landscapes.

buildings in terms of their footprint, height, number of storeys, year of construction and type, can also be used to construct 3D models [20-21]. However, as these GIS databases are mainly owned by local governments, their availability may be restricted by data privacy and relevant data policies.

The Light Detection and Ranging (LiDAR) technology is another method usable for constructing 3D geometry models. It typically utilizes laser light projected onto object surfaces and captures the reflected backscattering to generate 3D point clouds [22]. Upon 3D point clouds, a Digital Surface Model (DSM) representing the highest feature elevations, and a Digital Terrain Model (DTM) representing the bare-ground surface can be generated. Then, a normalized Digital Surface Model (nDSM), which provides a representation of the heights of above ground features, can be formed by subtracting the DTM from the DSM [23-24]. With the acquired nDSM, building footprints [25] and building heights [26] are capable of being extracted. To effectively use this method, it is essential to acquire reliable LiDAR data. Some agencies have provided these data for the public free of charge, however, their low resolution affects 3D models' accuracy [26]. Additionally, though some LiDAR data have high resolution [27], their availability and cost still need some concerns.

The last method that has been used to generate 3D geometry models for cities is the oblique photogrammetric technology, which employs Unmanned Aerial Vehicles (UAVs) to generate colored point clouds with a number of aligned aerial images and then processes the generated point clouds into textured building models [28-30]. Innovative technology though it is, this method is somewhat limited in the application

of generating 3D geometry models for cities due to several reasons. The first is the high cost of equipment required. In addition, flying UAVs may be restricted due to airspace regulations varying from country to country. In some countries like China, it is challenging and even impossible for researchers without a specific permission to fly UAVs over an entire city district to take oblique photographs. Lastly, the limited controlling range of UAVs is a hindrance as well.

The WWR data is also significant to 3D geometry models [8], however, its accurate determination is not an easy task. Since existing GIS databases hardly contain actual WWRs, researchers have to define WWR for all buildings under investigation, based on their knowledge, experience and judgement [11]. This practice may bring significant difference to exact conditions in terms of both solar heat gain and heat transfer loss [17].

As discussed above, existing methods creating 3D geometry models for UBEMs all have their limitations. To tackle these challenges, this study has developed a systematic approach acquiring building-relevant geometric data, namely building footprint, building height and WWR. The approach takes advantage of open-access data and Artificial Intelligence (AI) and does not require expensive equipment. Therefore, it provides researchers and practitioners with an innovative and effective method to create 3D geometry models for urban energy analysis using UBEMs.

The structure of this paper is as follows: Section 2 describes the developed approach acquiring relevant geometric data of individual buildings; Section 3 evaluates the performance of the developed approach in terms of its accuracy; Section 4

demonstrates the use of the newly developed approach using on an actual urban district; Section 5 offers appropriate and critical discussions on the investigated subject, and finally, Section 6 summarizes the main findings from this study.

2. Approach Development

2.1. Building footprint determination

High Resolution Remote Sensing (HRRS) images have been popularly to extract building footprint through clustering algorithms [31] and deep learning techniques [32-33]. Although the method provides adequate accuracy and completeness, it is still hindered from broad application due to the high cost of acquiring HRRS images.

In this study, two open data sources, namely Baidu Map (BDM) and OpenStreetMap (OSM), were used to determine footprints of buildings, following the process shown in Fig. 1, which includes three steps: 1) footprint extraction from BDM; 2) footprint extraction from OSM, and 3) combination of BDM and OSM building footprints. In this process, the use of OSM is to supplement missing components from the BDM, which are mainly big shopping centers as they are shown in BDM as indoor scenes which are not downloadable for geometry determination [34].

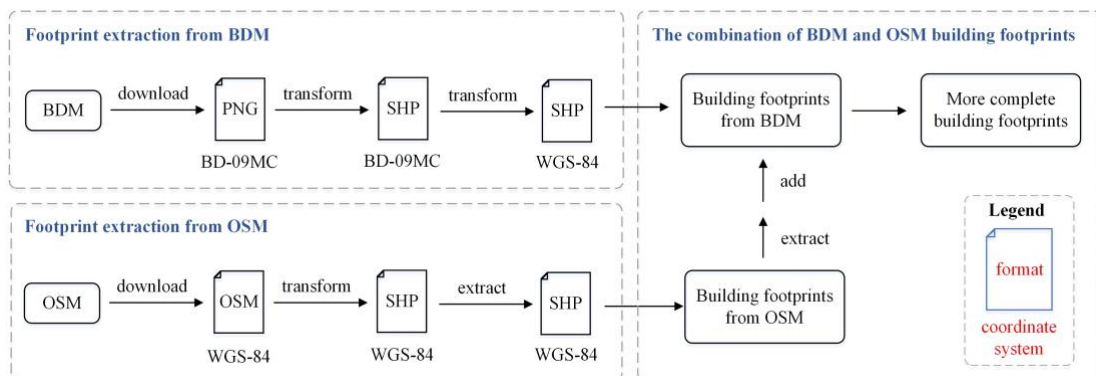


Fig. 1. Flowchart of building footprint determination.

2.1.1. Footprint extraction from BDM

BDM is a virtual map and geographical information program developed by Baidu Ltd, a major Internet company in China. In April 2010, Baidu announced that the API (Application Programming Interface) of BDM were open to the public for free. To use the API, users need to apply for one key in advance at [35]. The API creates maps based on URL parameters sent through a standard HTTP request and returns the maps as an image. Using the API, the “style” parameter, which defines the presentation of specific features, like roads, grasslands, rivers and building footprints, can be changed optionally within the map. Through a set of “style” operations to select the user-needed features, a styled map can be generated. Therefore, building footprints can be retrieved from styled maps by the API [36].

The building footprints were finally acquired in PNG format and BD-09MC² coordinate system through the API. Since the most commonly used format and coordinate system in geo-processing are SHP and WGS-84³, respectively, it is necessary to conduct image vectorization and coordinate transformation. Image vectorization was realized through a series of automatic operations in ArcMap, a commonly used program to display and explore GIS data [37], including “Resample”, “Reclassification”,

² BD-09MC, or BD-09 Mercator, is a projected coordinate system which was produced by Baidu in 2009, mainly serving for Baidu Map.

³ WGS-84, the abbreviation of World Geodetic System 84, is a universal geographic coordinate system which was defined in 1984. It is famous for the application of Global Positioning System (GPS).

“ArcScan” and “Simplify Polygon”. Among, “Resample” and “Reclassification” were the preparation for image vectorization, which were used to change the spatial resolution of input raster images and conduct binary processing, respectively. “ArcScan” was the key issue of this process that converted raster images into vector-based feature layers. “Simplify Polygon” was employed to remove redundant polylines and made vectored building footprints more simplified. Coordinate transformation was achieved by adjusting the coordinate system of vertices of building footprints, from BD-09MC to BD-09⁴, then GCJ-02⁵ and finally WGS-84. Fig. 2a displays the extracted building footprints in the WGS-84 coordinate system and SHP format, ready for further processing.

2.1.2. Footprint extraction from OSM

OSM is a free and editable digital map of the world. It is created, maintained and updated by a group of volunteers [38-39]. OSM is globally popular for its high shape accuracy and data update frequency [40]. However, its completeness varies significantly not only among countries, but also within countries [41]. The OSM digital map can be directly downloaded from its official website [42]. Then, the downloaded map in OSM format was transformed into SHP format through the website [43].

In OSM, there are four data layers, i.e., *points*, *lines*, *multilinestrings* and

⁴ BD-09 is the corresponding geographic coordinate system of BD-09MC. It was adjusted from GCJ-02.

⁵ GCJ-02 is a kind of geographic coordinate system which was adjusted from WGS-84 by National Administration of Surveying, Mapping and Geo-information of China in 2002.

multipolygons, with the *Points* layer referring to bus and train stations, the *Lines* and *multilinestrings* layers representing to highway and bus routes, respectively, and the *Multipolygons* layer denoting buildings and lands. To distinguish buildings from lands, three tags in *multipolygons*, namely *building*, *office* and *shop*, could be further specified. Therefore, if an object was linked with one of these three tags, it could be determined as a building. The building footprint extracted from OSM was in the WGS-84 coordinate system, awaiting further geo-analysis. Fig. 2b illustrates a sample of building footprint extracted from OSM.

2.1.3. *The combination of BDM and OSM building footprints*

Comparing the image of BDM building footprints (Fig. 2a) with that of OSM (Fig. 2b), it could be found that although most building footprints in the two images can match each other, there do exist some discrepancies (blue shows unique buildings produced from BDM; red shows unique buildings produced from OSM; green shows those buildings produced from both methods). Therefore, combining the information presented in both Fig. 2a and Fig. 2b would help to provide a more complete building footprint. Due to the characteristic of giving better completeness in building footprint [34], BDM was chosen as the base map, to which the extracted building footprints merely existing in OSM were added for final combination, as shown in Fig. 2c. This method can provide a good accuracy and this will be shown and discussed in Section 3.1.



Fig. 2. Building footprint determination process (a: extracted building footprints from BDM; b: extracted building footprints from OSM; c: combination of a and b).

2.2. Building height determination

In this part, a systematic method with flexibility and low cost has been proposed for both residential and non-residential buildings. It follows the process shown in Fig.

3.

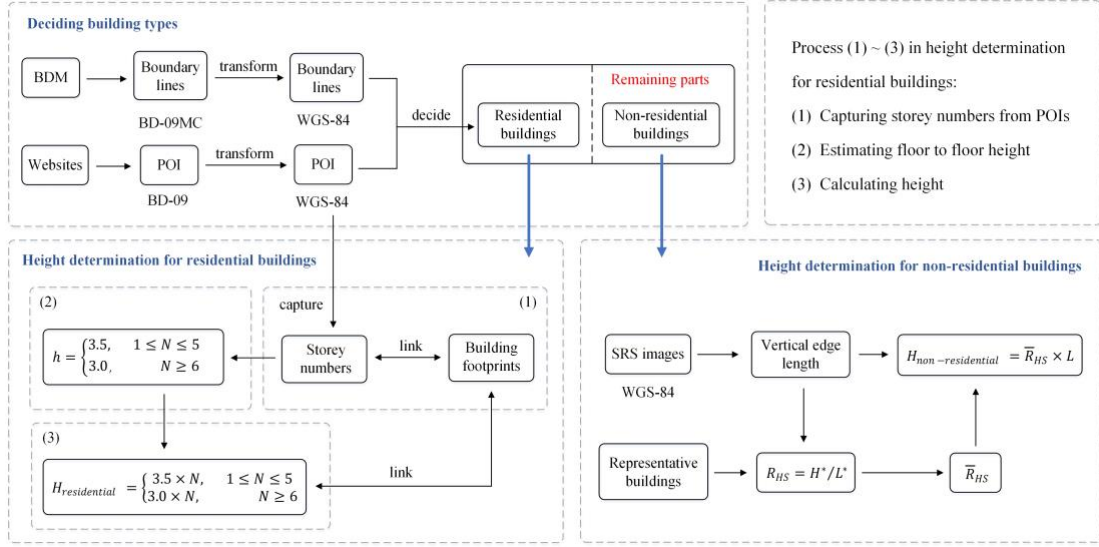


Fig. 3. Flowchart of building height determination.

2.2.1. Deciding building types

The height of residential buildings can be easily calculated by multiplying the number of storeys and the floor to floor height, as their floor to floor height is relatively fixed [44]. However, this phenomenon does not happen often for non-residential buildings. Therefore, it is of significance to distinguish residential buildings from non-residential buildings, before deciding the building height.

It is generally believed that the buildings within the boundary lines of residential communities are defined as residential buildings. Thus, as the precondition of determining residential buildings, it is necessary to acquire corresponding boundary lines. They can be acquired from BDM by the API in the BD-09MC coordinate system, which is of necessity to be transformed into the WGS-84 coordinate system for further use. Fig. 4a shows an example of residential buildings enclosed by corresponding boundary lines of residential communities.

For those residential buildings not located in any residential communities, their identification was through Points of Interests (POIs), which were formed by

downloading the information of names, the number of storeys, longitude and latitude from commercial rental websites [34], and then generating points in ArcMap through “Display XY data”. The POIs were acquired in the BD-09 coordinate system, which would then be transformed to the WGS-84 coordinate system. As shown in Fig. 4b, the locations of acquired POIs could be divided into two: 1) those inside the boundary lines of residential communities, and 2) those outside boundary lines but linked with a building. These buildings (highlighted in green in Fig. 4b) are also residential buildings. Except all residential buildings highlighted in Fig. 4b, all remaining buildings are considered as non-residential buildings.

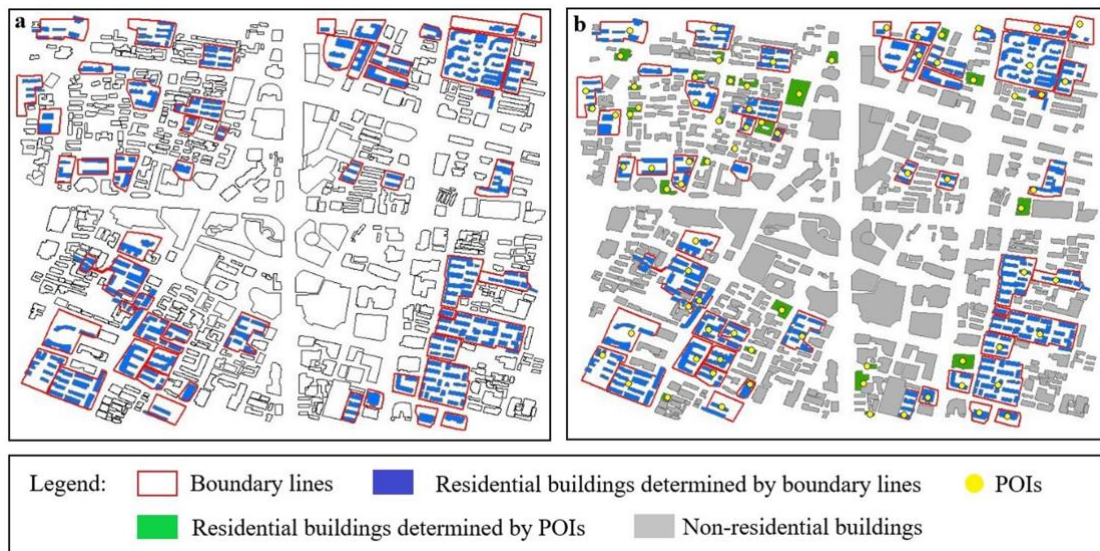


Fig. 4. A sample of residential buildings determination (a: determination through boundary lines; b: determination through POIs).

2.2.2. Height determination for residential buildings

(1) Capturing storey numbers from POIs

As discussed above, the information about the storey number was stored in POIs, which has been proven to have high accuracy [34]. The following step would capture

this information from POIs, and link them with building footprints. As the locations of POIs were divided into two kinds (inside and outside residential communities), and those buildings inside might have consistent storey number or not, the capturing method was developed into three types accordingly.

- For those inside residential communities and have consistent storey number (POIs have only one kind of storey number), the boundary lines were used to form boundary polygons firstly in the ArcMap through “Feature to Polygon”. Then, the storey number was captured from POIs, transferred to boundary polygons and building footprints in communities sequentially using “Spatial Join”. Because it is an automatic process, it saves time for acquiring storey numbers.
- For those inside residential communities with varying storey numbers (POIs have more than one kind of storey number), all buildings were checked manually to determine their storey numbers, based on the images from Baidu panoramic map [45], as shown in Fig. 5. Through the Baidu panoramic map, only a few buildings need to be visited on-site, hence reducing overall working time.
- For those outside residential communities, the information was captured from POIs and then directly linked to their building footprints, because they are individual buildings.



Fig. 5. Example building images from the Baidu panoramic map.

(2) Estimating floor to floor height

In China, there are two main kinds of residential buildings, i.e. houses and apartments. Generally, the storey number for houses is no more than five floors, with floor to floor height between 3.5m and 4.0m. For apartments, the minimum storey number is usually six, with floor to floor height between 2.8m and 3.0m. According to this, a building's floor to floor height (h in m) was determined by its storey number (N), acquired in the above session, using a tier-based algorithm with threshold set as five storeys, as defined in Eq. 1,

$$h = \begin{cases} 3.5, & 1 \leq N \leq 5 \\ 3.0, & N \geq 6 \end{cases} \quad (1)$$

(3) Calculating height

According to the floor to floor height and the number of storeys of each building, the i -th building's height was finally calculated by Eq. 2,

$$H_{residential,i} = h_i \times N_i = \begin{cases} 3.5 \times N_i, & 1 \leq N_i \leq 5 \\ 3.0 \times N_i, & N_i \geq 6 \end{cases} \quad (2)$$

2.2.3. Height determination for non-residential buildings

The storey number of non-residential buildings can be acquired through manual counting in the Baidu panoramic map as well. However, as their floor to floor heights are usually unfixed, the method developed in Section 2.2.2 cannot be used. On this occasion, another approach called building vertical edge method [46] was employed to estimate the heights of non-residential buildings. The method relies on Satellite Remote Sensing (SRS) images, and the building height equals to its vertical edge length in one SRS image (Fig. 6) multiplied by a ratio, as defined in Eq. 3 - 5.

$$H_{non-residential,i} = \bar{R}_{HS} \times L_i \quad (3)$$

$$\bar{R}_{HS} = \frac{1}{n} \cdot \sum_{i=1}^n R_{HS,i} \quad (4)$$

$$R_{HS,i} = H_i^* / L_i^* \quad (5)$$

where $H_{non-residential,i}$ is the height of the i -th non-residential building (in m); L_i is the vertical edge length of the i -th non-residential building (in m); \bar{R}_{HS} is the mean value of $R_{HS,i}$; $R_{HS,i}$ is the ratio of the i -th representative building; H_i^* is the height of the i -th representative building (in m), and L_i^* is the vertical edge length of the i -th representative building (in m).

An advantage of this method is that in SRS images, building vertical edges are unlikely to overlap even in high-density urban areas containing many high-rise buildings. The SRS images can be acquired from the Google Earth free of charge, in the WGS-84 coordinate system [46]. However, as the Google Earth is not available in China, a free map integration software called LocaSpace Viewer (LSV) [47] has been

employed to call the Google Earth. The vertical edge lengths of both target and representative buildings were manually measured from SRS images using the function of “Measurement” in ArcMap. The heights of representative buildings, which could be either residential or non-residential, were obtained from relevant records, such as Information websites and government reports. Furthermore, it should be noted that the dimension of SRS images should be less than 50km, in both east to west direction and south to north direction, so that the R_{HS} could be considered as a constant value [46]. Otherwise, a new R_{HS} should be calculated.



Fig. 6. Example building vertical edges in SRS images.

2.3. WWR determination

Accurate WWRs are usually difficult to acquire, especially at urban scale [11]. To quickly determine WWR for a large number of urban buildings with adequate accuracy,

an AI has been developed and trained, as shown in Fig. 7.

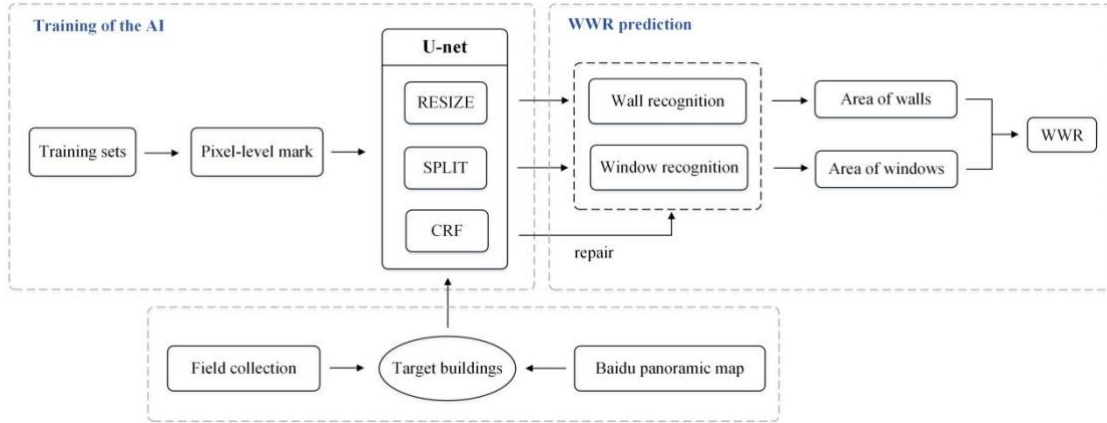


Fig. 7. Flowchart of WWR determination.

2.3.1. Algorithm of the AI

The algorithm employed by the AI is the U-net, which was originally developed for medical imaging processing [48]. Its architecture consists of two parts, namely a contracting path and an expansive path. The contracting path follows the typical architecture of a convolutional network and is used for semantic segmentation [49], that is extracting a group of image pixels belonging to a distinct object or category. The expansive path is used for restoring corresponding image pixels. The U-net has very good performance on image segmentation applications, and it is suitable for small sample models, with reasonable training time [48].

2.3.2. Functional modules of the AI

The AI consists of three main functional modules, namely RESIZE, SPLIT and CRF (Conditional Random Fields). RESIZE is for recognizing exterior walls in images containing a building elevation. SPLIT is for distinguishing windows from opaque parts

of walls. CRF is for repairing missing parts of either walls or windows caused by blocking obstacles, such as trees. The former two modules run for every building elevation image while the latter one only runs when a blocking obstacle is identified in the image.

2.3.3. *Training the AI*

After setting up the AI using the U-net framework, the next step was to train it to be able to recognize opaque walls and transparent windows in building elevation images. The training set was built with certain number of images containing various building elevations. The image selection was based on the following criteria:

- Covering a broad range of building types and ages, wall types and window types;
- Avoiding block from objects like trees, vehicles and other buildings.

The chosen images for training the AI algorithm were then marked with pixel-level precision, that is manually marking the walls and windows in the images as shapes containing a certain number of pixels. Although this operation seems to be time-consuming and labor-intensive, it can be done speedily by an image mark-up software, called *Colabeler* [50]. Since the U-net framework requires identical format and size of input images, all images used for training were compressed or resized to 512x512 pixels.

2.3.4. *Predicting WWR*

After training, the AI was able to recognize all walls and windows from one building elevation image. Fig. 8 illustrates a building elevation image (8a) and the recognized wall (8b) and all windows (8c) by the AI algorithm. The area of walls and

windows were automatically calculated by the AI, and WWRs could then be acquired.

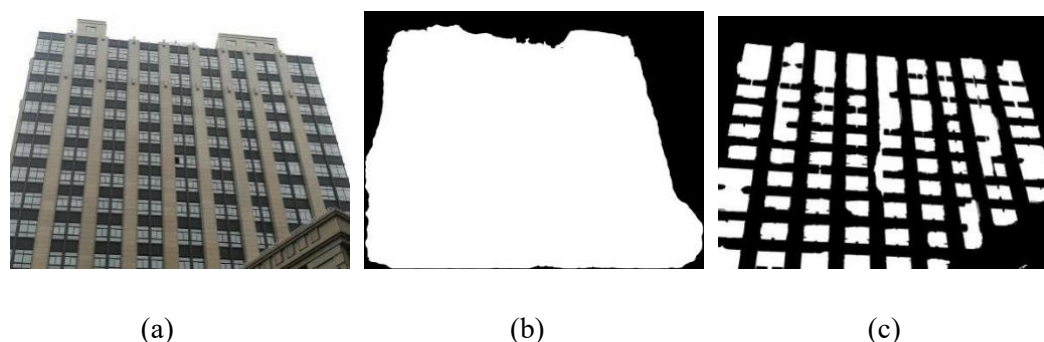


Fig. 8. Image recognition by the AI algorithm (a: original image; b: recognized wall; c: recognized windows).

The images needed for all target buildings within a district or urban were collected by two different methods. One method was taken directly from the Baidu panoramic map – this work can be combined with the storey number counting for certain residential buildings and non-residential buildings, and another was taken manually on-site, especially for those unavailable in the Baidu panoramic map.

3. Evaluation and Analysis

To test the approach developed in this study, the Nanjing City in China has been selected. It is the capital city of Jiangsu Province in China, and has over 8 million people, located in the Yangtze River Delta region. The administrative area of Nanjing is 6,587km², with urban built-up area of 1,399km² in 2017 compared with 513km² in 2005 [51], representing its rapid urbanization. According to China's climatic zoning [52], the local climate of Nanjing is categorized as 'hot summer and cold winter'. In addition,

two Central Business Districts (CBDs) in the city, namely Xinjiekou CBD⁶ and Hexi CBD⁷, were employed for benchmarking building footprints in Section 3.1 and a case study in Section 4, respectively. Fig. 9 illustrates the geographic locations of Nanjing in China and the two CBDs in Nanjing.

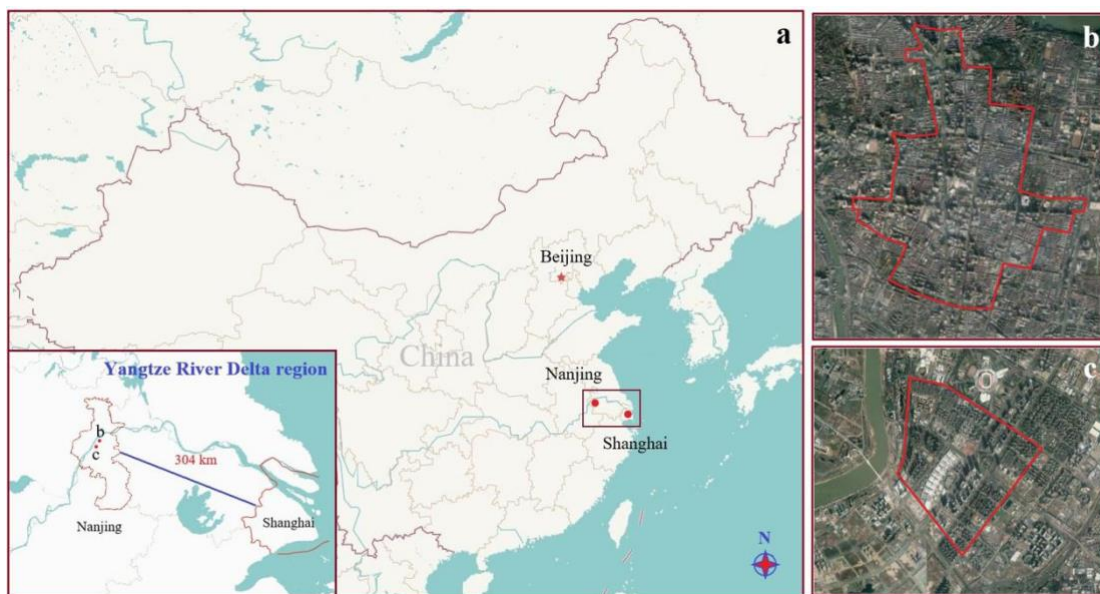


Fig. 9. The geographic location of (a: Nanjing; b: Xinjiekou CBD; c: Hexi CBD).

To quantify the accuracy of the developed method, four error metrics were employed, namely Error (E), Relative Error (RE), Mean Absolute Error (MAE) and Root Mean Square Error (RMSE), which could be calculated as Eq. 6 - 9.

$$E(X, h) = h(x_i) - y_i \quad (6)$$

⁶ Xinjiekou CBD is one of the most famous business districts in China, with a history of more than one hundred years. It covers an area of 5.6 km² and contains large numbers of banks and shopping malls.

⁷ Hexi CBD has been an important national financial agglomeration area since 2008, which undertakes the function of finance, exhibition, culture and commerce. In addition, it is also the second largest CBD in East China.

$$RE(X, h) = (h(x_i) - y_i)/y_i \quad (7)$$

$$MAE(X, h) = \frac{1}{m} \cdot \sum_{i=1}^m |h(x_i) - y_i| \quad (8)$$

$$RMSE(X, h) = \sqrt{\frac{1}{m} \cdot \sum_{i=1}^m (h(x_i) - y_i)^2} \quad (9)$$

where $h(x_i)$ represents the acquired value, and y_i denotes the true value.

3.1. Building footprint

To test the performance of predicting building footprint, the Xinjiekou CBD has been used, as it has a High Resolution Surveying Map (HRSM) produced in 2018 by a commercial mapping service corporation, so can be used as benchmark. Fig. 10 illustrates the footprints of all buildings in the Xinjiekou CBD, both acquired from the HRSM and predicted by the method presented in Section 2.1. The following sections will analyze from completeness and shape accuracy, respectively.

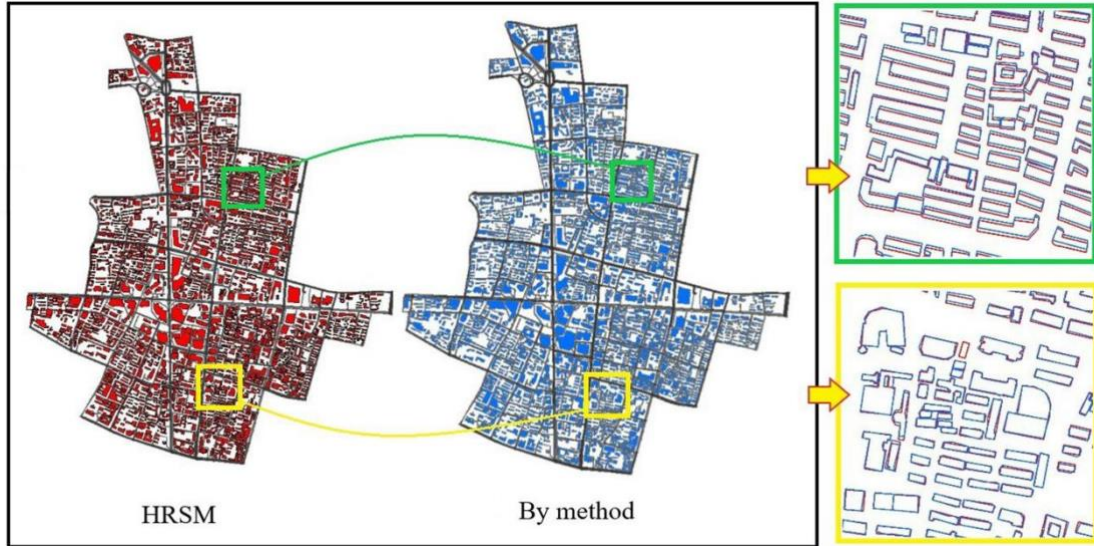


Fig. 10. Building footprints of the Xinjiekou CBD of Nanjing acquired from HRSM and those using the developed method, together with their comparison.

(1) Completeness

The HRSM in Fig. 10 contained a total of 2,370 building footprints, and this number dropped to 2,334 when predicted by the method presented in Section 2.1, with a difference of 1.52% only, reflecting a high level of completeness.

(2) Shape accuracy

The two zoomed in images in Fig. 10 visually reflected that the method developed in this study could accurately reproduce the shapes of building footprints, as comparing with those from the HRSM. To quantitatively describe their accuracy, Fig. 11 and Fig. 12 illustrate the distribution of errors of both building footprint area and perimeter.

As shown in Fig. 11a, the top three errors of area were in the range of -60m^2 and 40m^2 , and the MAE and the RMSE were 28.47m^2 and 40.05m^2 , respectively. From Fig. 11b, it could be found that 54% (33% + 21%) of the acquired building footprints had relative errors of area between -5% and +5%. Additionally, 86% (33% + 21% + 23% + 9%) of acquired building footprints showed relative errors of area between -10% and +10%. Overall, less than 15% of acquired building footprints had relative errors of the area, in terms of its absolute value, larger than 10%.

When doing an error analysis for perimeter, the errors for most samples were between -10m and 5m (Fig. 12a). Moreover, both MAE (4.57m) and RMSE (6.90m) were thought acceptable, as the mean perimeter in this region was 162.95m, which was calculated by the ArcMap. As shown in Fig. 12b, more than 90% (94%: 16% + 55% + 21% + 2%) of building footprints had them less than 10%, in terms of the absolute value. In conclusion, the acquired building footprints can well match the benchmark values from the HRSM, in terms of both area and perimeter.

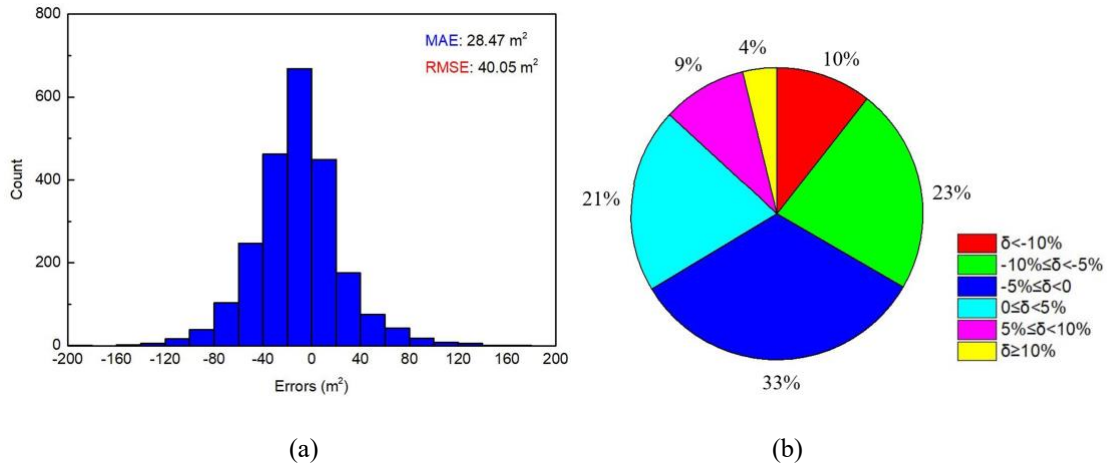


Fig. 11. The error analysis of area of the acquired building footprints (a: the distribution of errors, as well as MAE and RMSE; b: the distribution of relative errors).

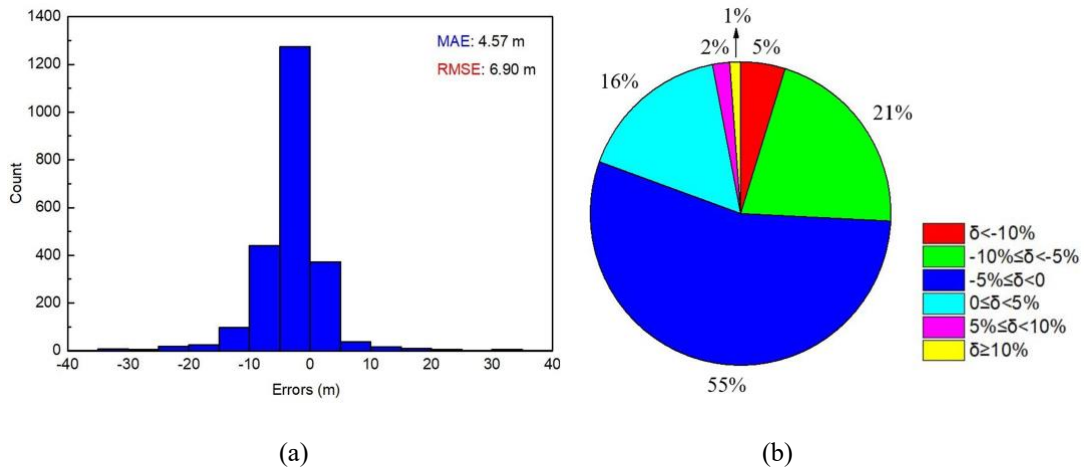


Fig. 12. The error analysis of perimeter of the acquired building footprints (a: the distribution of errors, as well as MAE and RMSE; b: the distribution of relative errors).

3.2. Building height

To evaluate the accuracy of the building height determined by the method presented in Section 2.2, *Energy efficiency evaluation reports of civil buildings in Jiangsu Province*⁸ were employed, as they contain actual number of storeys, height

⁸ Collected from multiple agencies in Jiangsu Province, i.e. government departments and architectural design institutes.

and WWR of some buildings (both residential and non-residential) in Nanjing.

(1) Residential buildings

In this test, one hundred residential buildings in Nanjing were randomly selected to estimate the accuracy of the method developed in Section 2.2.2, for acquiring height of residential buildings. Similar to the footprint, four error metrics were employed to quantify its accuracy.

As shown in Fig. 13a, the errors of height were within a range of -6m and 5m, and most errors were between -2m and 2m. The MAE (1.77m) was low and the RMSE (2.61m) indicated that there was no significant exception in the acquisition process. From Fig. 13b, 58% (29% + 29%) of acquired building heights showed very low relative errors between -5% and 5%, and 87% (29% + 29% + 22% + 7%) of acquired building heights showed low relative errors, with absolute values less than 10%, indicating good prediction performance.

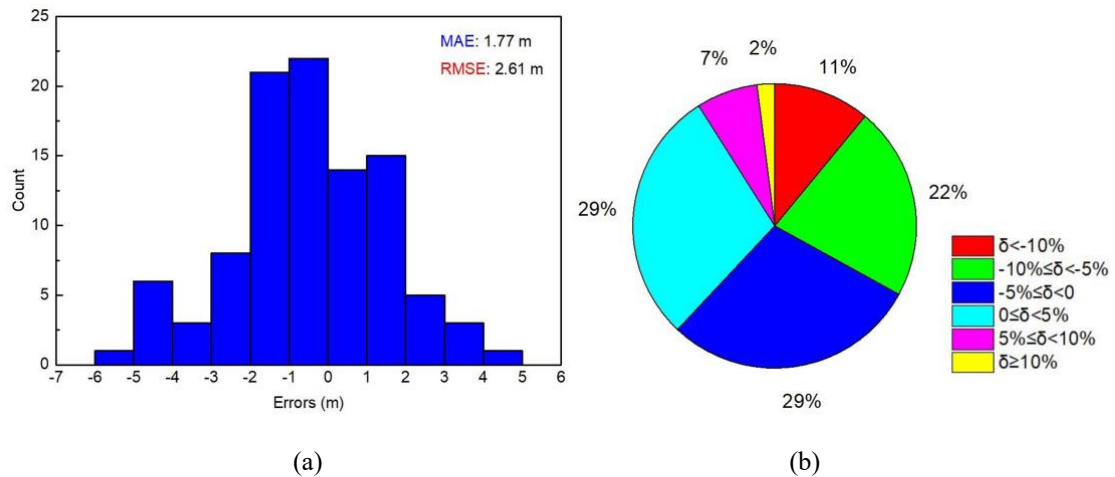


Fig. 13. The error analysis of the acquired building heights for residential buildings (a: the distribution of errors, as well as MAE and RMSE; b: the distribution of relative errors).

(2) *Non-residential buildings*

In Nanjing, 34 non-residential buildings, distributed within a region with a distance from east to west of 6.5km and a span from north to south of 8km, were selected to evaluate the performance of the method of acquiring height of non-residential buildings developed in Section 2.2.3. The selection of the region meets the distance requirement of less than 50km for using building vertical edge method [46]. Firstly, four buildings in this region were selected as representative buildings to calculate the \bar{R}_{HS} , based on Eq. 4 - 5. The results are shown in Table 1.

Table 1. The R_{HS} and \bar{R}_{HS} of representative buildings.

ID	H (m)	L (m)	R_{HS}	\bar{R}_{HS}
1	42.00	4.41	9.52	9.56
2	195.40	20.39	9.58	
3	58.80	6.15	9.56	
4	144.80	15.12	9.58	

The heights were acquired from *Energy efficiency evaluation reports of civil buildings in Jiangsu Province*.

Then, the vertical edge length of other 30 non-residential buildings were measured in a SRS image from the Google Earth, using the LSV, and their building heights were calculated by Eq. 3.

Fig. 14a demonstrates the distribution of errors for acquired heights, showing that most non-residential buildings had errors between -4m and 8m, with the MAE of 5.06m and the RMSE of 7.09m. From Fig. 14b, over half predictions (53%: 40% + 13%) had very low relative error within the range of -5% and 5%, and 74% (40% + 13% + 13% + 8%) of predicted building heights had low relative errors that were less than 10% in

terms of their absolute values.

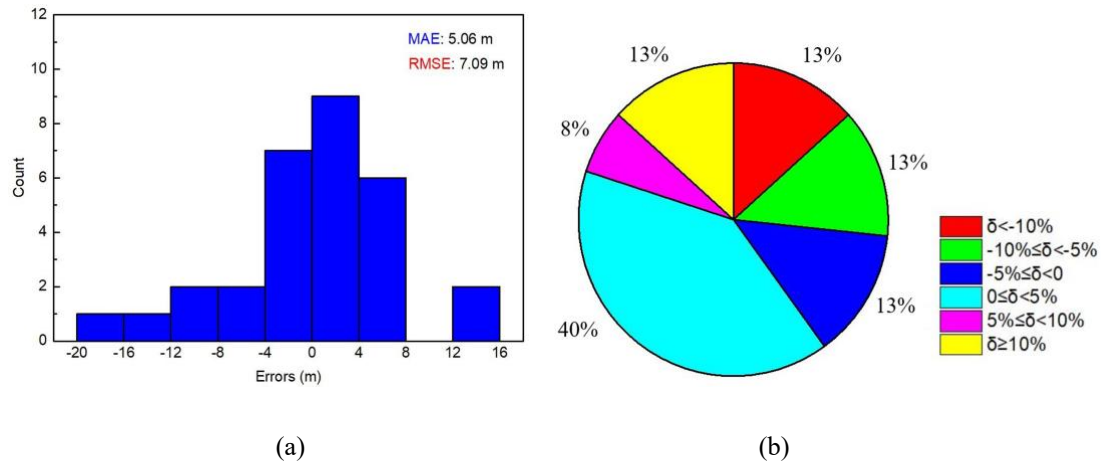


Fig. 14. The error analysis of the acquired building heights for non-residential buildings (a: the distribution of errors, as well as MAE and RMSE; b: the distribution of relative errors).

3.3. WWR

To decide WWRs, the AI algorithm mentioned in Section 2.3 was firstly trained with 150 elevation images collected in Nanjing city. Another 60 elevation images with accurate WWRs acquired from *Energy efficiency evaluation reports of civil buildings in Jiangsu Province* were then selected to validate the accuracy of the AI algorithm.

Fig. 15a illustrates the distribution of errors, as well as the MAE (0.07) and the RMSE (0.09). It shows that most acquired WWRs were within the range of 0 and 0.05, followed by the range of -0.05 and 0, and the range of -0.1 and -0.05. When considering the relative errors (Fig.15b), it could be observed that 75% (18% + 22% + 25% + 10%) of acquired WWRs had moderate relative errors between -10% and +10%, with 47% (25% + 22%) within the band of 5%.

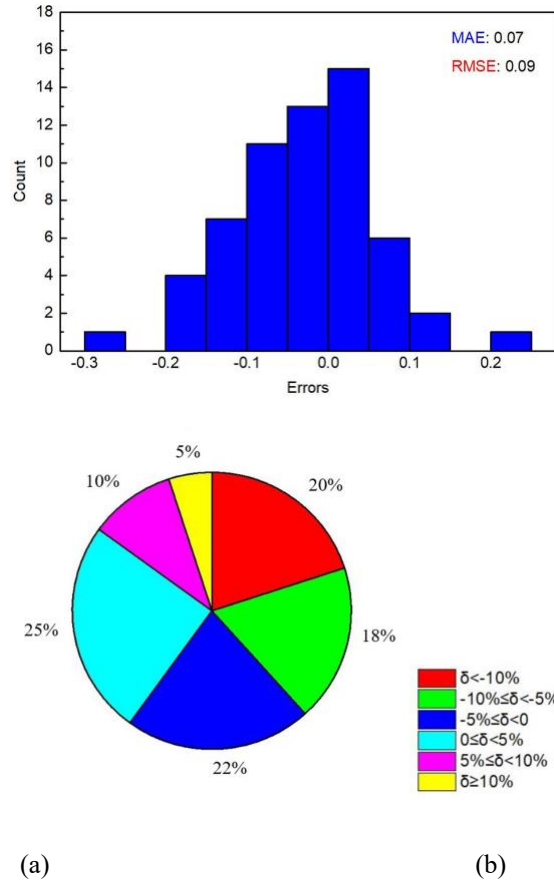


Fig. 15. The error analysis of the acquired WWRs (a: the distribution of errors, as well as MAE and RMSE; b: the distribution of relative errors).

4. Case study

Section 3 has well justified the usability and accuracy of the approach developed in this study. To demonstrate how to use it, the approach has been applied to the Hexi CBD (as shown in Fig. 9c), which is a newly developed urban district with an overall area of 4.5km², and this section introduces some major results.

From this practice, the geometric information of 400 buildings within the district was obtained, and Table 2 has listed the results of 10 typical buildings, including their footprint, height and the WWRs of different facades.

Based on the geometric information collected by the approach, a 3D model of the

Hexi CBD was built up in Grasshopper, a plugin to the CAD environment Rhinoceros 3D [18], as shown in Fig. 16a. In the model, 272 buildings were categorized as residential buildings, with the remaining 128 buildings categorized as non-residential buildings (Fig. 16b).

Table 2. The geometric information of 10 typical buildings.

ID	Building footprint (m²)	Building height (m)	WWR_E	WWR_W	WWR_S	WWR_N
1	775.43	33	0.16	0.16	0.27	0.27
2	485.43	17.5	0.17	0.17	0.38	0.38
3	923.04	54	0.29	0.29	0.50	0.47
4	982.86	21	0.18	0.18	0.36	0.36
5	16217.12	16	0.25	0.16	0	0
6	1295.52	144	0.88	0.88	0.88	0.88
7	1880.80	54.7	0.61	0.58	0.69	0.60
8	1434.89	175	1	1	1	1
9	4008.93	122.7	0.39	0.55	0.66	0.70
10	2611.70	176	1	1	1	1

WWR_E, WWR in the East; WWR_W, WWR in the West; WWR_S, WWR in the South; WWR_N, WWR in the North.

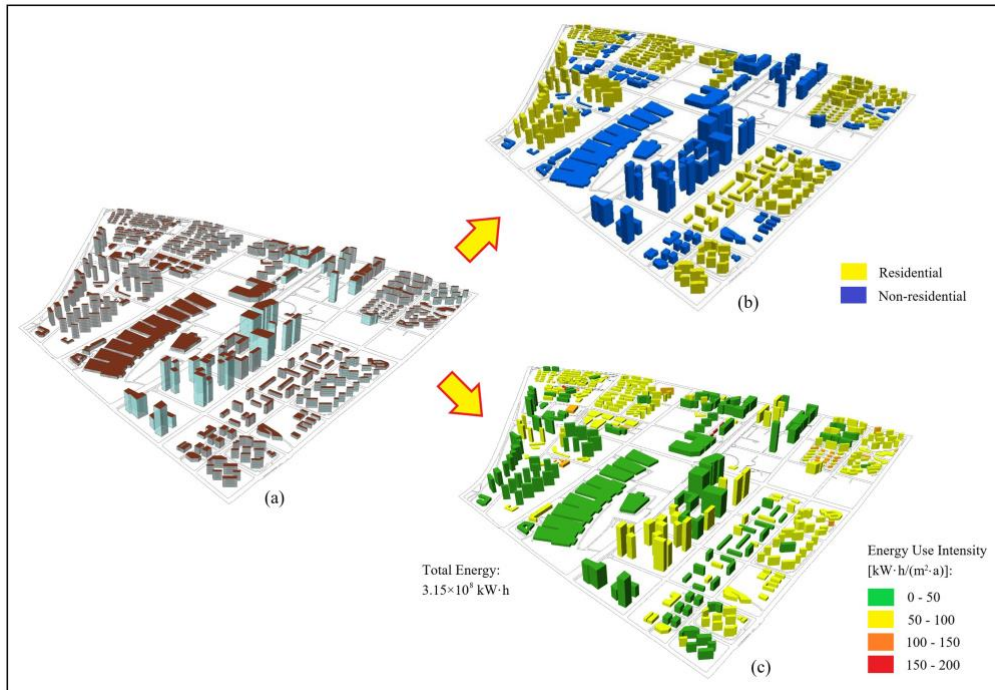


Fig. 16. The 3D model and energy prediction results for the Hexi CBD (a: urban 3D modeling; b: type determination; c: energy simulation).

Table 3 lists some statistical parameters for the 400 buildings in the Hexi CBD. From the Table, it could be observed that in the area under investigation, the mean building footprint area was 765.9m² for residential buildings, and this value was smaller than the 2972.75m² for non-residential buildings. The average building height was bigger than 40m (approximately 13 floors) for both residential and non-residential buildings, with a maximum value bigger than 120m (approximately 40 floors) for very tall buildings. Residential buildings showed bigger WWRs in south and north facades, comparing with the other two facades. This phenomenon, however, was not applicable to non-residential buildings, which had similar WWRs among facades. Because some non-residential buildings use glass curtain walls, their identified WWRs could reach 1.

Table 3. Statistical parameters for the 400 buildings in the Hexi CBD.

	Residential buildings			Non-residential buildings		
	Mean	Max	Min	Mean	Max	Min
Building footprint (m ²)	765.90	4643.83	239.40	2972.75	32579.38	145.06
Building height (m)	40.97	129	10.50	49.08	204	5
WWR_E	0.18	0.51	0.01	0.49	1	0
WWR_W	0.18	0.51	0.01	0.48	1	0
WWR_S	0.39	0.86	0.18	0.48	1	0
WWR_N	0.38	0.86	0.18	0.50	1	0

WWR_E, WWR in the East; WWR_W, WWR in the West; WWR_S, WWR in the South; WWR_N, WWR in the North.

The established 3D model can then be used for predicting building energy consumption at urban levels, using EnergyPlus, which is a global acknowledged simulation engine for building performance [53]. In fact, for accurate prediction of building performance, a 3D model, non-geometric data and weather data are all needed of being defined accurately [8]. However, in this study, the main purpose of this demonstration is to show how the established 3D model can help to do building performance simulation, but not producing accurate prediction results. Therefore, residential and non-residential buildings were merely set up using existing templates from ASHARE, for *Apartment* and *Open Office*, respectively [54]. And climate conditions were defined in the Typical Meteorological Year (TMY) file *CHN_Jiangsu.Nanjing.582380_CSWD*.

Fig. 16c has depicted grouped buildings based on their simulated energy consumption levels. According to the simulation results, the total annual energy consumption within this district was found to be 3.15×10^8 kW·h, for heating and

cooling the buildings inside. This value can be used by energy-policy makers to decide the energy efficiency of the district [55-56]. Additionally, grouping of buildings according to their energy levels may guide development of district energy distribution solutions and optimization [57]. Thirdly, the predicted energy consumption levels of individual buildings could be compared with benchmark values provided by government, e.g. 50 kW·h/(m²·a) for residential buildings and 100 kW·h/(m²·a) for office buildings [58], to identify those buildings need energy improvement. According to the predicted results in Fig. 16c, the residential buildings in yellow, orange and red, and the non-residential buildings in orange and red need special attentions on energy renovation.

According to existing studies, the 3D model developed here can also be used in other applications, such as Urban Heat Island (UHI) [59-61], zone ventilation [62-64], landscape planning [65-67] and flood prevention [68-69].

5. Discussions

5.1. Applicability to large scale districts

The approach introduced in this paper can be used for modeling hundreds or thousands of buildings, such as the cases of the Hexi CBD and the Xinjiekou CBD. However, it is still challenging of building up large-scale models targeting tens of thousands of buildings or even more. Main barriers include counting of storey number for residential buildings, measurement of vertical edge length for non-residential buildings, and image collection for WWR prediction, as all these tasks require some

manual efforts, which can be significant when the number of buildings under investigation is large.

Fortunately, the urban 3D modeling is a one-time task. Once the model is established, it can serve a variety of purposes. Therefore, spending time, labor and resources to establish a complete 3D geometric model is worthwhile. Another observation is that many UBEMs reported merely employ hundreds or thousands of buildings [13-15], a scale that the proposed method is capable of handling.

5.2.Applicability to world-wide cities

BDM is confirmed to offer a fairly accurate and complete building footprint dataset in China. However, its applicability to cities outside of China has not been tested yet. Google Map is reported to have abilities to extract building footprints in some other countries [26]. Therefore, a mode of “Google Map + OSM” may work in the future.

The method to acquire building heights for residential buildings has been tested in other parts of China and the results have suggested its usability, due to the availability of both community boundaries and POIs. However, the availability of these data may be different in other countries, due to factors like government policies and culture, and this has to be confirmed before the method is used in other countries. In addition, the sources, like Google Map and local websites, may be suitable replacements in these countries. Unlike residential buildings, the method developed for non-residential buildings is believed to be more applicable to world-wide cities. One of the reasons is that satellite images are nowadays widely available for most major cities in the world.

One can easily access these images via Google Earth and other similar service providers.

For the method predicting building's WWRs, it is independent on the city and country under investigation as long as building elevation images can be collected.

5.3. Time and cost

It does not take much time to acquire building footprints since downloading maps from the OSM and the BDM is fast (for thousands of buildings, no more than 15 minutes). Some manual efforts are needed in the process such as coordinating transformation and image vectorization. However, even with this extra time needed, the overall process of acquiring building footprints is still fairly efficient.

The time required for deciding the height of residential buildings is shared by two tasks. Task 1 is acquisition of boundary lines and POIs. For a model with thousands of residential buildings, this task although takes several hours to complete, but most work can be completed automatically. Task 2 is the manual counting of storey number, with an efficiency around 60 ~ 120 buildings/(hour·person).

To decide the height of non-residential buildings, the measurement of the vertical edge length is relatively slow, as each building was measured three times to ensure their accuracy. The efficiency is tested as 30 ~ 60 buildings/(hour·person).

A longer time is devoted to collecting images for predicting WWR. In one field practice, a team of five people completed on-site image collection for about 400 buildings within 2 days (8 working hours a day). Thus, the efficiency is estimated as 10 buildings/(hour·person). On this basis, we believe that the efficiency can still be improved in cases where some building elevation images are expected to be acquired

from the Baidu panoramic map.

Regarding to cost, the proposed approach relies on openly accessible datasets. No special equipment and skills are needed, except computers and cameras.

5.4. Accuracy and further improvements

Although the accuracy of this approach has been justified in Section 3, there are still further possible improvements that can make the approach more accurate, summarized as followings:

- It should be acknowledged that some residential buildings may be classified as non-residential buildings mistakenly, as they belong to no residential communities or contain no POIs. Therefore, a method that can identify these residential buildings is needed in the future to improve the identification accuracy.
- For height determination of residential buildings, year of construction can be employed as another variable in Eq. 1, as this value may be updated along with the development of relevant building design standards [70].
- Subjective determination of vertical edge length by human eyes may cause errors, and this process requires certain manual labour. Therefore, it is of great significance to employ AI technics to automatically extract the vertical edge length. In addition, as a test showed that the building vertical edge method also had good accuracy on residential buildings (20 samples, MAE: 1.51, RMSE: 3.33), the improved method that uses the AI may be applied to all building types.
- For WWR determination, it is worthy of trying other AI algorithms to see the possibility of promoting accuracy on recognizing walls and windows, as well as

repairing those missing parts in elevation images.

6. Conclusions

3D models of buildings are fundamental for urban building energy modeling. However, in many countries, its establishment is limited to the existence of GIS databases or the access of existing GIS databases. Additionally, its establishment is also prevented by the availability of reliable LiDAR data, and the restricted use of flying UAVs. To tackle these issues, an innovative and convenient approach has been proposed in this study, which can acquire accurate geometric data about buildings, including their footprints, heights and WWRs.

- The determination of building footprints is achieved based on data collected from two online platforms, namely, the BDM and the OSM. The former platform is used as the basis and the latter platform is used to provide missing buildings in the former one, especially shopping centers. The accuracy of this method has been validated and the validation results showed that the MAE and the RMSE for the area were 28.47m^2 and 40.05m^2 , respectively, and the values were 4.57m and 6.90m for the perimeter. In addition, more than 85% of acquired building footprints had absolute relative errors less than 10%.
- The determination of building height is achieved for residential buildings and non-residential buildings, separately. For residential buildings, the height is calculated by multiplying number of storeys and floor to floor height, with the number of storeys acquired from commercial rental websites and the floor to floor height

estimated according to the obtained number of storeys. For non-residential buildings, the building vertical edge measured on SRS images is employed to determine building height, based on the calculated \bar{R}_{HS} of representative buildings. The accuracy of this method has been validated and the validation results showed that the MAE was 1.77m and 5.06m, and the RMSE was 2.61m and 7.09m for residential and non-residential buildings, respectively. Besides, 87% (residential) and 74% (non-residential) of acquired building heights had absolute relative errors less than 10%.

- The determination of WWRs is automatically carried out by an AI algorithm consisting of three main functional modules, namely RESIZE, SPLIT and CRF, based on elevation images taken either onsite or from the Baidu panoramic map. The accuracy of this method has been validated and the validation results showed that 75% of acquired WWRs had absolute relative errors less than 10%, with the MAE of 0.07 and the RMSE of 0.09.

To demonstrate the use of this method in real applications, a case study has been carried out for a newly developed CBD in Nanjing, with a total area of 4.5km². Using the approach introduced here, a 3D geometric urban model has been developed for the district, with easily identified residential and non-residential buildings from all 400 buildings. Additionally, the use of building energy simulation to all these buildings provided useful information about the energy demand from all buildings within the district to help policy makers optimize district energy performance.

Lastly, possible future work directions from this study may include:

- Confirming the usability of some resources, such as Google Map and local rental websites, in other countries, as some resources used in this study are only available in China.
- Developing the AI algorithm to automatically extract building vertical edge length to avoid potential errors by human eyes, as well as speeding up the process of measurement.
- Developing more advanced algorithms for predicting WWR with better accuracy, and testing its usability in more cities.

Declarations of interest

None.

Acknowledgements

This paper is financially supported by the National Key R&D Program of China (grant number: 2017YFC0702302).

References

- [1] U. Al-mulali, Factors affecting CO₂ emission in the Middle East: a panel data analysis, *Energy* 44 (1) (2012), 564–569.
- [2] T. Schuetze, J.-W. Lee, T.-G. Lee, Sustainable urban (re-)Development with building integrated energy, water and waste systems, *Sustainability* 5 (3) (2013), 1114-1127.

- [3] United Nations-Habitat, Energy, 2017 (Accessed on 5 September, 2017), <http://unhabitat.org/urban-themes/energy/>.
- [4] San Francisco Environment, San Francisco, Citywide Greenhouse Gas Reduction Actions and Goals, 2018 (Accessed on 10 March, 2018), <https://sfenvironment.org/article/citywide-actions-and-goals>.
- [5] Greater London Authority, Mayors Energy Strategy and Climate Change Action Plan – Action Today for Protection Tomorrow, 2004.
- [6] Beijing Municipal People's Government, Beijing's work plan for energy conservation and climate change response under the guidelines of the 13th five-year national plan, 2016.
- [7] Shanghai Municipal People's Government, Shanghai's work plan for energy conservation and greenhouse gas emission reduction under the guidelines of the 13th five-year national plan, 2018.
- [8] C.F. Reinhart, C. Cerezo Davila, Urban building energy modeling—A review of a nascent field, *Building and Environment* 97 (2016), 196–202.
- [9] EIA, Annual Energy Outlook, 2016.
- [10] L. Parshall, K. Gurney, S.A. Hammer, D. Mendoza, Y. Zhou, S. Geethakumar, Modeling energy consumption and CO₂ emissions at the urban scale: methodological challenges and insights from the United States, *Energy Policy* 38 (9) (2010), 4765–4782.
- [11] C. Cerezo Davila, C.F. Reinhart, J.L. Bemis, Modeling Boston: A workflow for the efficient generation and maintenance of urban building energy models from existing geospatial datasets, *Energy* 117 (2016), 237-250.
- [12] Y. Chen, T. Hong, X. Luo, B. Hooper, Development of city building dataset for urban building energy modeling, *Energy and Buildings* 183 (2019), 252–265.
- [13] C. Cerezo Davila, N. Jones, A. Al-Mumin, A. Hajiah, C. Reinhart, Implementation of a calibrated Urban Building Energy Model (UBEM) for the evaluation of energy efficiency scenarios in a Kuwaiti residential neighborhood, in: *Proceedings of the 15th IBPSA Conference: San Francisco, USA, 2017*.

- [14] Y. Chen, T. Hong, M.A. Piette, Automatic generation and simulation of urban building energy models based on city-scale building retrofit analysis, *Applied Energy* 205 (2017), 323–335.
- [15] C.S. Monteiro, C. Costa, A. Pina, M.Y. Santos, P. Ferrao, An urban building database (UBD) supporting a smart city information system, *Energy and Buildings* 158 (2018), 244–260.
- [16] CityGML, [Online]. Available: <https://www.citygml.org/>.
- [17] R. Nouvel, M. Zirak, V. Coors, U. Eicker, The influence of data quality on urban heating demand modeling using 3D city models, *Computers, Environment and Urban Systems* 64 (2017) 68–80.
- [18] J. Sokol, C. Cerezo Davila, C.F. Reinhart, Validation of a Bayesian-based method for defining residential archetypes in urban building energy models, *Energy and buildings* 134 (2017), 11-24.
- [19] C. Wang, S. Tindemans, C. Miller, G. Agugiaro, J. Stoter, Bayesian calibration at the urban scale: a case study on a large residential heating demand application in Amsterdam, *Journal of Building Performance Simulation* 13(3) (2020), 347-361.
- [20] M. Österbring, É. Mata, L. Thuvander, M. Mangold, F. Johnsson, H. Wallbaum, A differentiated description of building-stocks for a georeferenced urban bottom-up building-stock model, *Energy and Buildings* 120 (2016), 78–84.
- [21] T. Dogan, C. Reinhart, Shoeboxer: An algorithm for abstracted rapid multi-zone urban building energy model generation and simulation, *Energy and Buildings* 140 (2017), 140–153.
- [22] K. Chen, W. Lu, F. Xue, P. Tang, L.H. Li, Automatic building information model reconstruction in high-density urban areas: Augmenting multi-source data with architectural knowledge, *Automation in Construction* 93 (2018), 22–34.
- [23] T. Partovi, F. Fraundorfer, R. Bahmanyar, H. Huang, P. Reinartz, Automatic 3-D Building Model Reconstruction from Very High Resolution Stereo Satellite Imagery, *Remote Sensing* 11(14) (2019), 1660.

- [24] M. Rodrigue, C.M.H. Demers, M. Parsaee, Lighting in the third dimension: laser scanning as an architectural survey and representation method, *Intelligent Buildings International* 2020, <https://doi.org/10.1080/17508975.2020.1745741>.
- [25] S. Sun, C. Salvaggio, Aerial 3D building detection and modeling from airborne LiDAR point clouds, *IEEE Journal of Selected Topics in Applied Earth Observations and Remote Sensing* 6 (3) (2013), 1440–1449.
- [26] C. Ren, M. Cai, X. Li, Y. Shi, L. See, Developing a rapid method for 3-dimensional urban morphology extraction using open-source data, *Sustainable Cities and Society* 53 (2020), 101962.
- [27] T.R. Tooke, N.C. Coops, J. Webster, Predicting building ages from LiDAR data with random forests for building energy modeling, *Energy and Buildings* 68 (2014), 603-610.
- [28] S.P. Singh, K. Jain, V.R. Mandla, A new approach towards image based virtual 3D city modeling by using close range photogrammetry, *ISPRS Annals of Photogrammetry, Remote Sensing and Spatial Information Sciences*, 2(5) 2014, 329-337.
- [29] Y. Li, S. Chen, X. Feng, 3D Modelling of Oversize Cities based on Oblique Photogrammetry: Key Technique Considerations and Experimental Results, in: proceedings of 5th International Workshop on Earth Observation and Remote Sensing Applications: Xi'an, China, 2018.
- [30] J. Liang, J. Gong, J. Liu, Y. Zou, J. Zhang, J. Sun, S. Chen, Generating Orthorectified Multi-Perspective 2.5D Maps to Facilitate Web GIS-Based Visualization and Exploitation of Massive 3D City Models, *International Journal of Geo-Information* 5(11) (2016), 212.
- [31] N. Gavankar, S.K. Ghosh, Object based building footprint detection from high resolution multispectral satellite image using K-means clustering algorithm and shape parameters, *Geocarto International* 34(6) (2018), 626-643.
- [32] H. He, J. Zhou, M. Chen, T. Chen, D. Li, P. Cheng, Building extraction from UAV images jointly using 6D-SLIC and multiscale Siamese convolutional networks, *Remote Sensing* 11(9) (2019), 1040.
- [33] Y. Zhang, W. Gong, J. Sun, W. Li, Web-Net: A novel nest networks with ultra-hierarchical sampling for building extraction from aerial imageries, *Remote Sensing* 11(16) (2019), 1897.

- [34] C. Wang, Y. Li, X. Shi, Information mining for Urban Building Energy Models (UBEMs) from two data sources: OpenStreetMap and Baidu Map, in: Proceedings of the 16th IBPSA Conference: Rome, Italy, 2019.
- [35] Baidu Map Open Platform, [Online]. Available: <http://lbsyun.baidu.com/>.
- [36] Baidu Map API, [Online]. Available: <http://lbsyun.baidu.com/index.php?title=static>.
- [37] ArcMap, [Online]. Available: <https://developer.baidu.com/map/custom/?qq-pf-to=pcqq.c2c>.
- [38] J. Schiefelbein, J. Rudnick, A. Scholl, P. Remmen, M. Fuchs, D. Muller, Automated urban energy system modeling and thermal building simulation based on OpenStreetMap data sets, *Building and Environment* 149 (2019), 630-639.
- [39] A. Alhamwi, W. Medjroubi, T. Vogt, C. Agert, OpenStreetMap data in modelling the urban energy infrastructure: a first assessment and analysis, in: Proceedings of the 9th International Conference on Applied Energy: Cardiff, UK, 2017.
- [40] H. Fan, A. Zipf, Q. Fu, P. Neis, Quality assessment for building footprints data on OpenStreetMap, *Journal of Geographical Information Science* 28(4) (2014), 700–719.
- [41] R. Goldblatt, N. Jones, J. Mannix, Assessing OpenStreetMap Completeness for Management of Natural Disaster by Means of Remote Sensing: A Case Study of Three Small Island States (Haiti, Dominica and St. Lucia), *Remote Sensing* 12(1) (2020), 118.
- [42] OpenStreetMap, [Online]. Available: <http://www.openstreetmap.org>.
- [43] GeoConverter, [Online]. Available: <https://geoconverter.hsr.ch/>.
- [44] Y. Wu, L.S. Blunden, A.B.S. Bahaj, City-wide building height determination using light detection and ranging data, *Environment and Planning B: Urban Analytics and City Science* 46(9) (2019), 1741–1755.
- [45] Baidu panoramic map, [Online]. Available: <https://map.baidu.com/>.
- [46] F. Qi, J.Z. Zhai, G. Dang, Building height estimation using Google Earth, *Energy and Buildings* 118 (2016), 123–132.
- [47] LocaSpace Viewer. Available: <http://www.locaspace.cn/>.
- [48] O. Ronneberger, P. Fischer, B. Thomas, U-net: Convolutional Networks for Biomedical Image Segmentation, in: proceedings of 18th International Conference on Medical Image Computing and Computer-Assisted Intervention: Munich, Germany, 2015.

- [49] A. Garcia-Garcia, S. Orts-Escolano, S.O. Oprea, V. Villena-Martinez, J. Garcia-Rodriguez, A review on deep learning techniques applied to semantic segmentation, *Transactions of Pattern Analysis and Machine Intelligence* (2017), arXiv:1704.06857.
- [50] Colabeler. Available: <http://www.colabeler.com/>.
- [51] Nanjing Statistic Bureau, Nanjing municipal bureau statistics 2017, 2017.
- [52] GB 50176-2016, Code for thermal design of civil building, 2016.
- [53] EnergyPlus. Available: <https://www.energyplus.net/>.
- [54] ASHARE Standard 90.1-2013, Energy Standard for buildings except low residential buildings, 2013.
- [55] R. Choudhary, Energy analysis of the non-domestic building stock of Greater London, *Building and Environment* 51 (2012), 243-254.
- [56] P. Mouzourides, A. Kyprianou, M. K.-A. Neophytou, J. Ching, R. Choudhary, Linking the urban-scale building energy demands with city breathability and urban form characteristics, *Sustainable Cities and Society* 49 (2019), 101460.
- [57] A. Omu, R. Choudhary, A. Boies, Distributed energy resource system optimisation using mixed integer linear programming, *Energy Policy* 61 (2013), 249-266.
- [58] GB 51161-2016, Standard for energy consumption of building, 2016.
- [59] C. Guo, R. Buccolieri, Z. Gao, Characterizing the morphology of real street models and modeling its effect on thermal environment, *Energy and Buildings* 203 (2019), 109433.
- [60] P. Bhiwapurkar, D. Moschandreas, Street geometry and energy conservation of urban buildings in Chicago, *Intelligent Buildings International* 2(4) (2010), 233-250.
- [61] Y. Xu, C. Ren, P. Ma, J. Ho, W. Wang, K.K.L. Lau, H. Lin, E. Ng, Urban morphology detection and computation for urban climate research, *Landscape and Urban Planning* 167 (2017), 212-224.
- [62] J. Yang, S. Jin, X. Xiao, C. Jin, J. Xia, X. Li, S. Wang, Local climate zone ventilation and urban land surface temperatures: Towards a performance-based and wind-sensitive planning proposal in megacities, *Sustainable Cities and Society* 47 (2019), 101487.

- [63] A. Ricci, I. Kalkman, B. Blocken, M. Burlando, A. Freda, M.P. Repetto, Large-scale forcing effects on wind flows in the urban canopy: Impact of inflow conditions, *Sustainable Cities and Society* 42 (2018), 593-610.
- [64] D.J. Wise, V.B.L. Boppana, K.W. Li, H.J. Poh, Effects of minor changes in the mean inlet wind direction on urban flow simulations, *Sustainable Cities and Society* 37 (2018), 492-500.
- [65] S. Zhu, S. Du, Y. Li, S. Wei, X. Jin, X. Zhou, X. Shi, A 3D spatiotemporal morphological database for urban green infrastructure and its applications, *Urban Forestry & Urban Greening* 58 (2021), 126935.
- [66] Z. Tang, Y. Ye, Z. Jiang, C. Fu, R. Huang, D. Yao, A data-informed analytical approach to human-scale greenway planning: Integrating multi-sourced urban data with machine learning algorithms, *Urban Forestry & Urban Greening* 56 (2020), 126871.
- [67] Y. Ye, W. Zeng, Q. Shen, X. Zhang, Y. Lu, The visual quality of streets: A human-centred continuous measurement based on machine learning algorithms and street view images, *Environment and Planning B – Urban Analytics and City Science* 46(8) (2019), 1439.
- [68] H. Darabi, B. Choubin, O. Rahmati, A.T. Haghighi, B. Pradhan, B. Klove, Urban flood risk mapping using the GARP and QUEST models: A comparative study of machine learning techniques, *Journal of Hydrology* 569 (2019), 142-154.
- [69] S. Yamashita, R. Watanabe, Y. Shimatani, Smart adaptation activities and measures against urban flood disasters, *Sustainable Cities and Society* 27 (2016), 175-184.
- [70] C. Delmastro, G. Mutani, S.P. Corgnati, A supporting method for selecting cost-optimal energy retrofit policies for residential buildings at the urban scale, *Energy Policy* 99 (2016), 42-56.